UNIVERSITY OF LEEDS

This is a repository copy of *Numerical assessment of changes in land–atmosphere interactions during the rainy season in South America using an updated vegetation map*.

White Rose Research Online URL for this paper:
https://eprints.whiterose.ac.uk/id/eprint/213210/

Version: Accepted Version

**Article:**

Talamoni, I.L. orcid.org/0000-0003-4952-190X, Kubota, P.Y., Cavalcanti, I.F.A. orcid.org/0000-0002-3890-5767 et al. (3 more authors) (2024) Numerical assessment of changes in land–atmosphere interactions during the rainy season in South America using an updated vegetation map. International Journal of Climatology, 44 (10). pp. 3278-3294. ISSN 0899-8418

https://doi.org/10.1002/joc.8523

© 2024 Royal Meteorological Society. This is the peer reviewed version of the following article: Numerical assessment of changes in land–atmosphere interactions during the rainy season in South America using an updated vegetation map, which has been published in final form at https://doi.org/10.1002/joc.8523. This article may be used for non-commercial purposes in accordance with Wiley Terms and Conditions for Use of Self-Archived Versions. This article may not be enhanced, enriched or otherwise transformed into a derivative work, without express permission from Wiley or by statutory rights under applicable legislation. Copyright notices must not be removed, obscured or modified. The article must be linked to Wiley's version of record on Wiley Online Library and any embedding, framing or otherwise making available the article or pages thereof by third parties from platforms, services and websites other than Wiley Online Library must be prohibited.

**Reuse**

Items deposited in White Rose Research Online are protected by copyright, with all rights reserved unless indicated otherwise. They may be downloaded and/or printed for private study, or other acts as permitted by national copyright laws. The publisher or other rights holders may allow further reproduction and re-use of the full text version. This is indicated by the licence information on the White Rose Research Online record for the item.

**Takedown**

If you consider content in White Rose Research Online to be in breach of UK law, please notify us by emailing eprints@whiterose.ac.uk including the URL of the record and the reason for the withdrawal request.

White Rose
university consortium
Universities of Leeds, Sheffield & York

eprints@whiterose.ac.uk
https://eprints.whiterose.ac.uk/

# NUMERICAL ASSESSMENT OF CHANGES IN LAND-ATMOSPHERE INTERACTIONS DURING THE RAINY SEASON IN SOUTH AMERICA USING AN UPDATED VEGETATION MAP

Isabella L. Talamoni[1], Paulo Y. Kubota[1], Iracema F. A. Cavalcanti[1], Dayana C. de Souza[1], Jessica C. A. Baker[2], Rita M. S. P. Vieira[3]

[1]Centro de Previsão de Tempo e Estudos Climáticos (CPTEC), Instituto Nacional de Pesquisas Espaciais – INPE, Cachoeira Paulista, Brazil

[2]School of Earth and Environment, Institute for Climate and Atmospheric Science, University of Leeds, Leeds, UK

[3] Centro de Ciência do Sistema Terrestre, Instituto Nacional de Pesquisas Espaciais - INPE, São José dos Campos, Brazil

Corresponding author: Isabella L. Talamoni, e-mail: isabella.lima@inpe.br

Keywords: Rainy Season; Land Use and Land Cover Change; Atlantic Forest; IBIS; BAM.

Funding: *Coordenação de Aperfeiçoamento de Pessoal de Nível Superior* - CAPES (process 88887.354679/2019-00) associated with CLIMAX-FAPESP-Belmont-2015/50687-8 and CNPq – Project 306393/2018-2.

## Abstract

Land Use and Land Cover Change (LULCC) is a key driver of changes in land-atmosphere interactions, playing an essential role in climate and weather patterns in South America (SA). This study used a modelling approach to assess the land-atmosphere changes introduced by LULCC over the Brazilian territory. Numerical experiments of early (2006), neutral (2004), and late (2008) rainy season onset years were performed in the Integrated BIosphere Simulator (IBIS) to assess the land-surface parameters, and in Brazilian Atmospheric Model (BAM) to assess the atmospheric variables. The models were run with a natural (NAT) vegetation map and an updated (UP) vegetation map, which incorporated realistic Brazil deforestation up to the early 2000s. The differences between the two maps were particularly larger over 25-15°S and 50-40°W, where the Atlantic Forest and Cerrado biomes were replaced by pasture. IBIS experiments showed that over the area of larger LULCC there was an increase in albedo of up to 8% while reductions in net radiation, surface heat fluxes, surface temperature, and surface roughness were noticed. Land-atmosphere feedbacks assessed with BAM experiments showed that LULCC contributed to a drier and colder (stable) atmosphere over central-east SA that opposes the necessary conditions for the rainy season onset. The changes included increases in surface pressure and low-level wind associated with reductions in 2 m temperature and surface roughness. These changes contributed to decrease the cloud formation and less precipitation in all three rainy season onset years, but particularly in the late rainy season onset year during September-October-November (SON). The atmospheric changes induced by LULCC show a pattern of dry atmosphere (reduced precipitation), similar to those of late onset years, and indicate that LULCC enhances the late rainy season onset condition over central-east SA. Additionally, this study highlights the importance of considering up-to-date vegetation maps because these changes significantly affect both surface and atmospheric variables.

**Keywords:** Rainy Season; Land Use and Land Cover Change; Atlantic Forest; IBIS; BAM.

## 1. Introduction

The South American Monsoon System (SAMS; Zhou and Lau, 1998; Gan et al., 2004; Vera et al., 2006; Marengo et al., 2012; De Carvalho and Jones, 2016) is a prominent seasonal variability mode comprising all the central and east areas of South America (SA). It is characterized by well-defined annual dry and rainy seasons (Gan et al., 2004). SAMS seasonal variability is often verified through the reversal of the low-level circulation monthly anomalies (wind annual mean remotion), and through the seasonal shift in precipitation and Outgoing Longwave Radiation (OLR) over SA (Zhou and Lau, 1998, Gan et al., 2004). Although SAMS is one of the main contributors to the rainy season in SA, herein we consider the rainy season as the period when persistent precipitation is established over the central and east areas of SA (Liebmann and Marengo, 2001; Bombardi et al., 2019).

Different methodologies were developed to identify the rainy season onset, but they all converge to the onset between mid-October and mid-November over the SA northwest region, gradually extending southeastward and reaching the precipitation peak between December and February (Kousky, 1988; Liebmann and Marengo, 2001; Gan et al., 2004; Silva and Carvalho, 2007; Raia and Cavalcanti, 2008; Nieto-Ferreira and Rickenbach, 2011).

Local forcings, such as Land Use and Land Cover Change (LULCC), contribute to the SA rainy season. Modeling studies have shown that circulation and precipitation variabilities in particular SA rainy season regions, such as the southern Amazon, are primarily influenced by local factors rather than remote ones (Marengo et al., 2003; Fu and Li, 2004; Xue et al., 2006; Ma et al., 2011). Additionally, the evaporation at the end of the dry season over the Amazon region has been pointed out as triggering mechanism to SAMS onset (Li and Fu, 2004). Therefore, land-atmosphere interactions are a local forcing that plays an important role in climate and weather of SA (Collini et al., 2008; Da Rocha et al., 2009; Souza, 2009; Aragão, 2012; Khanna et al., 2017). LULCC has become a prominent study subject due to its direct impact on both local and regional climates (e.g., Yang and Dominguez et al., 2019). Studies have established a link between deforestation and the rainy season onset delay in the southern Amazon (Butt et al., 2011; Debortoli et al., 2015; Leite-Filho et al., 2019). Chambers and Artaxo (2017) attributed the delay in rainy season onset to changes in surface roughness. Furthermore, deforestation has been linked to reduced precipitation due to evapotranspiration and moisture transport decrease (Spracklen and Garcia-Carreras, 2015; Spracklen et al., 2018), as well as temperature increase over the southern Amazon (Rezende et al., 2022). Wright et al. (2017) identified an important mechanism involving the link between the Amazon Forest transpiration and the increase in shallow convection during the dry to rainy-season transition. This moisture pumping through shallow convection is considered a precondition to the rainy season onset. These studies motivate the hypothesis explored in our present study that LULCC affects the rainy season in SA.

LULCC presents a major threat to natural biomes. In 2021, only 12.4 % of the original Atlantic Forest (Southeast and south of Northeast regions of Brazil) was still preserved (SOS Mata Atlantica, 2021). Since LULCC modifies land-atmosphere interactions, it is essential to provide realistic and up-to-date vegetation maps in both land-surface and Atmospheric General Circulation Models (AGCM) to ensure accurate simulations (Cavalcanti et al., 2017). In the present study, an offline framework with the Integrated BIosphere Simulator (IBIS; Kubota, 2012) was used to assess the land-surface parameters, while an online framework with the Brazilian Atmospheric Model (BAM; Figueroa et al., 2016; Lima, 2021) was used to assess the atmospheric variables. These frameworks were employed to investigate how LULCC affects the surface and atmospheric variables during the SA rainy season. An updated vegetation map was implemented into IBIS and BAM to assess, respectively, the surface and atmospheric sensitivity to LULCC. These numerical modelling experiments provide insights into how LULCC affects the SA rainy season and what is the importance of considering LULCC in AGCMs. The updated vegetation map included LULCC over the Brazilian territory with historical deforestation that occurred up until the early 2000s, particularly the replacement of the Atlantic Forest and Cerrado.

## 2. Data and Methods

### 2.1 Data

Table I provides a detailed overview of the data utilized in this study. The initial condition of IBIS-OFFLINE experiments was data from the Global Land Data Assimilation System which is a rain gauge and satellite-based dataset (GLDAS; Beaudoing and Rodell, 2020). ERA5 reanalysis hourly data (Hersbach et al., 2023) was used as the initial condition for BAM 3D experiments. The boundary condition over the oceans in BAM 3D experiments was from the NCEP – NOAA sea surface temperature data (Huang et al., 2020). Additionally, the initial soil water content conditions were derived from GLDAS.

### 2.2 Rainy season onset years selection

Talamoni et al. (2022) developed a methodology using the Rainy And Dry Season (RADS; Bombardi et al., 2019) global dataset to identify years marked by early and late rainy season onsets in SA. The authors, calculated onset date anomalies using RADS and classified years as early (late) onset based on whether the percentage of negative (positive) onset date anomalies in central SA exceeded 60% (Talamoni et al., 2022). Neutral rainy season onset was determined by a nearly 50% percentage in central SA. Based on these selection criteria, 2006 (September 30), 2004 (October 11), and 2008 (November 11) were selected as representative years for early, neutral, and late rainy season onsets, respectively. More details of early, neutral, and late onset years can be found in Talamoni et al. (2022). Figure 1 shows ERA5 variables (sea level pressure, moisture flux and wind at 850 hPa) and GPCP precipitation differences between the early and late onset years in the months of SON (September-October-November) and DJF (December-January-February). During SON and DJF, precipitation was greater over the northwest (central-east) SA in the late (early) onset year (Figure 1d, h). In SON, negative SLP differences were observed over Argentina and center-west of South Atlantic Ocean (Figure 1a) which indicates higher SLP in the late onset. Talamoni et al. (2022) investigated the development of a high SLP system in late onset years which was associated with atmospheric blocking episodes contributing to a delay in the rainy season onset. In DJF, negative SLP differences extended from the south Pacific to South Atlantic southward of 35°S (Figure 1e), indicating a predominance of lower pressure systems in extratropical latitudes in the early onset year compared to the late onset year, which may have played a role in the development of transient weather systems. During DJF, these systems acquire a stationary behavior that contributes to organizing the northwest-southeast precipitation band over SA called the South Atlantic Convergence Zone (SACZ; Kodama, 1992), which also explains the precipitation anomalies over the central-east SA in the early onset year (Figure 1h). SACZ is the main convective feature associated with SAMS. Its features can be identified by the northwesterly moisture flux that extends from the Amazon Basin towards the Southeast region of Brazil and the Atlantic Ocean. Figure 1f shows the enhanced moisture flux over central-east SA in the early onset year. This enhanced moisture flux is accompanied by enhanced 850-hPa wind speed across central SA (Figure 1g) meaning that more moisture is advected by the northwesterly flux. The intensity of the differences in Figure 1 is relatively high compared to climatology, in particular for precipitation and moisture flux.

## 2.3 Vegetation Maps

The two vegetation maps used in the numerical experiments for IBIS and BAM models are shown in Figure 2. The natural vegetation map (NAT) in Figure 2a uses IBIS vegetation classes (Foley et al., 1996) and has a spatial resolution of 0.5°x0.5°. NAT vegetation map is implemented in the Brazilian Atmospheric Model (BAM; Figueroa et al., 2016).

Figure 2b shows the Brazilian ProVeg map, an updated representation of vegetation cover and land use for the Brazilian territory derived from the ProVeg project (Vieira et al., 2013). This map is a result of satellite data and remote sensing techniques combined with geographic datasets and deforestation data from Environmental Programs such as PRODES and SOS *Mata Atlântica* for the early 2000s. The ProVeg project map has a spatial resolution of 1 km (0.01°x0.01°) (Vieira et al., 2013) and uses the SSiB vegetation scheme classes (Xue et al., 1991).

The updated vegetation map (UP) in Figure 2c was obtained from the merge between the Brazilian land cover map from the ProVeg project in Figure 2b and the NAT map in Figure 2a. To merge NAT and ProVeg vegetation maps, an algorithm to establish the relationship between the IBIS and SSiB vegetation classes was used. The relationship between these two model's vegetation classes is shown in Figure 2d. UP vegetation map has a spatial resolution of 0.5°x0.5° and uses IBIS vegetation scheme classes. The main differences between NAT and UP vegetation maps were particularly evident in the Atlantic Forest (Southeast and south of Northeast regions of Brazil) and the Cerrado (Northeast and Central-East regions of Brazil) biomes that were replaced by pasture in the UP vegetation map (Figure 2c).

## 2.4 IBIS-OFFLINE experiments

Global numerical experiments were performed using the land-surface model IBIS version Agro-IBIS 2.6b5 implemented by Kubota (2012). IBIS experiments were offline meaning that dynamic vegetation feedback from the land to the atmosphere was not assessed in this study. This approach is consistent with previous research conducted by Rezende et al. (2022) and Ruscica et al. (2022).

The vegetation parameters were obtained from model calibration studies with in-situ data (Imbuzeiro, 2005; Senna et al., 2009; Cunha et al., 2013; Araújo et al., 2016). For each rainy season onset year (early, neutral and late), two experiments were performed: one with the NAT vegetation map (Figure 2a) and the other with the UP vegetation map (Figure 2c). In total, six numerical experiments were performed over the simulation period from 1 July to 28 February of each respective rainy season onset year (Table 2). IBIS model was configured to a Gaussian grid resolution with triangular truncation of 126 waves (approximately 1°x1° of horizontal resolution).

**2.5 BAM 3D experiments**

AGCM experiments were performed to assess the land-atmosphere feedback due to LULCC. The AGCM used to perform the numerical experiments was the Brazilian Atmospheric Model (BAM; Figueroa et al., 2016) version 2.2.1 (Lima, 2021). BAM is a spectral model with hybrid vertical coordinates. Its dynamical core is a monotonic two-time-level semi-Lagrangian scheme, i.e., the tridimensional transport of moisture, microphysical (liquid water, ice, etc), and tracer prognostic variables (ozone, carbon dioxide) are solved at each grid point. BAM has ~1°x1° of horizontal resolution, i.e., triangular quadratic truncation with 126 waves and 42 vertical levels (from 1000 to 2 mb). Detailed configurations of the model's physical processes are in Table 3.

Table 4 shows the five experiments performed for each rainy season onset condition (early, neutral and late). The experiment's initial condition date varied from the first to the fifth day of the month, therefore, ensemble analyses were performed. Each experiment was performed for both vegetation maps, NAT and UP, thus, a total of ten experiments were obtained for each rainy season onset condition and for each simulation period (one from July to March and the other from October to May). The simulation period was split into two to guarantee a closer soil moisture initial condition from GLDAS. It ensures that the DJF simulation has a less dry moisture initial condition in October compared to the one in July. Thus, the July to March (October to May) simulation period was used for SON (DJF) analysis. DJF analysis was included due to differences between early and late rainy season onset years identified in Figure 1h and also by

Talamoni et al. (2022). Therefore, DJF analysis is relevant to assess if different rainy season onset dates can affect the rainy season period and its associated features.

### 2.6 t-Student test

Student's t statistical test (Spiegel, 1979) at a significance level of 5% was used to assess the differences between BAM 3D experiments with NAT and UP vegetation maps. The null hypothesis considered in the test was that changes in atmospheric variables were not related to LULCC. The critical value ($t$) was obtained from a two-tailed table with 8 degrees of freedom ($N_{NAT}+ N_{UP} - 2$). $N_{NAT}$ and $N_{UP}$ are the sample size, i.e., the number of BAM 3D experiments performed with each vegetation map ($N = N_{NAT}$=$N_{UP}$=5). $\mu_{NAT}$ and $\mu_{UP}$ are the NAT and UP experiments ensemble averages, respectively. $s_{NAT}$ and $s_{UP}$ are the standard deviation expressed by equation 3. The covariance coefficient ($\sigma$) was obtained by equation 2, and subsequently, the t-value ($t$) was determined by equation 1.

$$\begin{cases} t = \dfrac{\mu_{NAT} - \mu_{UP}}{\sigma\sqrt{\dfrac{1}{N_{NAT}} + \dfrac{1}{N_{UP}}}} & (1) \\ \sigma = \sqrt{\dfrac{N_{NAT}.s_{NAT}{}^2 + N_{UP}.s_{UP}{}^2}{N_{NAT} + N_{UP} - 2}} & (2) \\ s = \sqrt{\dfrac{\sum(X_i - \mu)^2}{N - 1}} & (3) \end{cases}$$

### 2.7 Water Budget

A surface water budget analysis was performed, similar to Talamoni et al. (2022). The objective was to differentiate the contribution of each water budget component in UP and NAT experiments. The water budget ($WB$) components shown in equation 4 are: the total vertically integrated water vapour flux divergence over the rectangular area ($C_w$), precipitation (P), evapotranspiration (E) and runoff (R). The rectangular area is the area between 25-15°S and 50-40°W. P is the total precipitation (kg $m^{-2}$ $day^{-1}$) and R is the runoff (kg $m^{-2}$ $day^{-1}$), both output variables from BAM. Likewise, the latent heat flux (LE) from surface (W $m^{-2}$) is an output from BAM. LE was converted to E as equation 5 (Allen et al., 1998) where $\lambda$ is the latent heat of vaporization at 25°C °C (2.4 x $10^6$ J $kg^{-1}$). E was converted from kg $m^{-2}$ $s^{-1}$ to mm $day^{-1}$.

To compute $C_w$, shown in equation 8, we employed box model calculations (Satyamurty et al., 2013) which is the sum of the vertically integrated water vapour flux divergence across the four walls over the area between 25-15°S and 50-40°W. $T_e$, $T_w$, $T_s$ and $T_n$ are the water vapour transport across the eastern, western, southern and northern walls, respectively. $C_w$ is in units of kg m$^{-2}$ s$^{-1}$, later converted to mm day$^{-1}$. It is also noteworthy that $C_w$ derives from Gauss's theorem which involves the divergence of the water vapor flux field over the rectangular area.

Initially, equation 6 was used to calculate both zonal ($qu$) and meridional ($qv$) vertically integrated water vapour fluxes (kg m$^{-1}$ s$^{-1}$; Brubaker et al., 1994). $u$ and $v$ are, respectively, the zonal and meridional wind components (m s$^{-1}$), $q$ is the specific humidity (kg kg$^{-1}$), $g$ is the gravitational constant (9.81 m.s$^{-2}$) and $p$ is the atmospheric pressure (kg m$^{-1}$ s$^{-2}$). The vertical integral considered the pressure levels between 3 (top of the atmosphere) and 1000 mb (surface). $u$, $v$ and $q$ are outputs of BAM.

The water vapour transport across the four walls $T_e$, $T_w$, $T_s$ and $T_n$ was computed using equation 7, which involves the line integral with integration limits defined by the latitudes ($lat$) and longitudes ($lon$) of the rectangular area.

$$WB = C_w + (P - E + R) \qquad (4)$$

$$E = \frac{LE}{\lambda} \qquad (5)$$

$$\begin{cases} qu = \dfrac{1}{g} \displaystyle\int_{p1=3}^{p2=1000} u \cdot q \, dp \\ qv = \dfrac{1}{g} \displaystyle\int_{p1=3}^{p2=1000} v \cdot q \, dp \end{cases} \qquad (6)$$

$$\begin{cases} T_{e\,(lon=-40)} = -\oint_{lat=-25}^{lat=-15} qu\,dy \\ T_{w\,(lon=-50)} = \oint_{lat=-25}^{lat=-15} qu\,dy \\ T_{n\,(lat=-15)} = -\oint_{lon=-50}^{lat=-40} qv\,dx \\ T_{s\,(lat=-25)} = \oint_{lon=-50}^{lat=-40} qv\,dx \end{cases} \quad (7)$$

$$C_w = T_w + T_e + T_s + T_n \quad (8)$$

## 3. Results

### 3.1 IBIS-OFFLINE experiments

NAT and UP vegetation maps were used to perform IBIS-OFFLINE experiments. Table 5 shows the mean difference between UP and NAT experiments over the area between 25-15°S and 50-40°W, where major LULCC occurred (Figure 2). Overall, similar changes were observed in early, neutral and late rainy season onset conditions due to LULCC:

a) Albedo increased by up to 8%, meaning that more shortwave radiation is reflected by the surface, resulting in lower temperatures with consequent decreases in longwave radiation emission by the surface. It is noteworthy that both incident shortwave and longwave radiation components were prescribed in IBIS-OFFLINE experiments. Once less energy is available on the surface, decrease in net radiation (shortwave and longwave net at the surface), sensible and latent heat fluxes and surface temperature were verified. The reduction in latent heat flux is attributed not only to the decreased energy available for soil water evaporation, but also to differences in the transpiration rates between C3 and C4 vegetation types. Specifically, C3 forest vegetation type (e.g., Atlantic Forest) has a higher transpiration rate compared to C4 pasture vegetation type (Taiz and Zeiger, 2010). Similar results were identified by Souza (2009) when the desertification was considered over the Semi-Arid Northeast region of Brazil and also by Oliveira (2008) when deforestation was considered over the east-Amazon. Evaporation reduction was also observed in LULCC offline experiments over the southern-Amazon by Rezende et al. (2022).

b) Soil water content decrease, although this reduction was relatively subtle. As an offline experiment, the primary forcing was the precipitation initial condition, which, in turn, was determined by the early, neutral, and late rainy season onset conditions.

### 3.2 BAM 3D experiments

The difference between UP and NAT experiments (BAM 3D) for early, neutral, and late onset years was analyzed over SA. Although LULCC is restricted within the Brazilian territory, BAM 3D analysis was extended to the SA domain. This expansion is justified by the effect perturbations such as LULCC have on remote regions through nonlinear interactions via atmospheric circulation. Similar effects of vegetation changes on remote regions have been identified in AGCM studies related to desertification in northeast Brazil (Oyama and Nobre, 20004) and to Amazon deforestation (Nobre et al., 2009).

To determine whether the differences between UP and NAT were attributed to LULCC, Student's t-statistical test at a 95% confidence level was applied. Positive (negative) differences indicate that the variable increased (decreased) in the UP experiment compared to the NAT experiment, i.e., UP > NAT (UP < NAT). Therefore, the following analysis mentions positive (negative) differences as an increase (decrease) of the variable due to LULCC.

In SON, precipitable water reduction (negative difference) was verified due to LULCC. This reduction was noticeable over the northeast and southeast regions of SA during early onset conditions (Figure 3a) and over the central-eastern part of SA in the case of late onset (Figure 3o), with the statistical significance covering a larger geographical area in the latter. As consequence there is a decrease of water vapor availability. This, in turn, can suppress both cloud formation and precipitation over the same region, specifically the central-eastern part of SA. Similar condition of precipitation reduction in BAM3D experiment was verified in Figure 1d, considering the GPCP difference between late and early onset.

An Outgoing Longwave Radiation (OLR) increase in UP experiments was simulated over the central-east SA, with statistical significance in all three early, neutral, and late onset years (Figure 3b, i, p). This OLR increase indicates a reduction in the formation of high-top clouds due to LULCC. Consequently, less precipitation is expected to occur over these areas. In the late onset, a statistically significant increase in OLR due to LULCC was verified across the central-east SA (Figure 3p), similar to the precipitable water reduction (Figure 3o). It implies that the northwest-southeast precipitation pattern, typically associated with the SACZ, weakens due to LULCC during late onset. The particular impact of LULCC in SACZ's life cycle is a gap for future studies that can be assessed with daily output simulations.

A statistically significant decrease in OLR was verified across the northern and northeastern regions of SA in the late onset year (Figure 3p). This decrease suggests a compensatory signal to the south, i.e., a weak northwest-southeast cloud and precipitation band. Therefore, these OLR differences exemplify the amplification of the precipitation reduction pattern over SACZ region during late onset year (Figure 3q) attributed to LULCC.

Precipitation reduction was verified over the study area and the central-northern SA in the early onset (Figure 3c), over the central-eastern SA in the neutral onset (Figure 3j), and over a portion of central and southeastern SA in the late onset (Figure 3q). To the south of the area with precipitation reduction, a precipitation increase was verified in all three onset years (Figure 3c, j, q), with statistical significance observed only during the late onset (Figure 3q). It indicates that LULCC had a suppressing (enhancing) effect on precipitation near the SACZ (La Plata Basin) domain. The enhanced precipitation over the La Plata Basin (Figure 3c, j, q) can be associated with the formation of transient systems with more stationary behavior, a phenomenon frequently observed during the rainy season, as reported by Raia and Cavalcanti (2008). In the late onset, a precipitation increase was also verified over the northwest SA (Figure 3q) which further reinforces the late onset pattern observed in GPCP data (Figure 1d).

A statistically significant increase in 850 hPa wind magnitude (Figure 3d, k, r) was observed over the central, eastern and northeastern SA areas (indicated by positive wind magnitude differences). This increase is associated with the SLP increase over central-east SA. An SLP increase means greater pressure gradient, thus, a wind acceleration. Additionally, the SLP increase can be linked to the displacement of the subtropical South Atlantic high-pressure system closer to the continent, further increasing the moisture transport from the ocean and the wind speed.

The increase in 850 hPa wind magnitude over SA can promote changes in the northwesterly moisture flux which in turn can modify the position of the precipitating systems associated with the rainy season such as the SACZ.

A statistically significant decrease in 2 m temperature was verified mainly over the central-east in the early, neutral and late onset (Figure 3e, l, s). This reduction of up to 2.5°C due to LULCC is attributed to the decrease in both net radiation and sensible heat flux simulated in the IBIS experiments.

Positive SLP differences were verified over the central-east SA in all early, neutral and late rainy season onset years (Figure 3f, m, t). However, these positive SLP differences were statistically significant only in the late onset year when they were verified throughout SA reaching the Atlantic Ocean between the coast of Argentina and the northeast coast of Brazil (Figure 3t). The statistically significant positive SLP differences indicate an SLP increase due to LULCC. The SLP increase over the Atlantic Ocean (along the coast of Argentina) has the potential to weaken transient systems that typically form in this cyclogenetic region (Gan and Rao, 1991; Reboita et al., 2010). These transient systems play an important role in enhancing both soil and atmospheric moisture (Raia and Cavalcanti, 2008; Talamoni et al., 2022), pre-conditioning the rainy season onset. They also contribute to organize the cloudiness band over the SA and the Atlantic Ocean (Raia and Cavalcanti, 2008). Therefore, weak transient systems can contribute to further delay the rainy season late onset condition.

The SLP increase (Figure 3f, m, t) reiterates the suppressed precipitation due to LULCC (Figure 3c, j, q). Consequently, an OLR increase is expected (Figure 3b, i, p). While an OLR increase may suggest a net radiation increase due to incident shortwave increase (cloud cover effect) it was not enough to offset the albedo increase contribution (due to LULCC). Therefore, a statistically significant decrease in net radiation of up to 30 W $m^{-2}$ (negative differences) is observed over the southeast SA (Figure 3g, n, u). The net radiation decrease is attributed to the albedo increase induced by LULCC. This effect was confirmed by IBIS-OFFLINE experiments (Table 5), which reveal an increase in incident shortwave radiation being reflected to the atmosphere.

In DJF, precipitable water decrease (negative difference) was simulated from northwest to central-east SA in neutral onset year (Figure 4h). In the early onset, the precipitable water decrease was shifted towards the north compared to the neutral onset (Figure 4a). The statistically significant OLR increase in UP experiments across the northwest and central-east in both early and neutral onset years (Figure 4a, h), reiterates the precipitable water decrease over this region. Therefore, it is possible to associate that the northwest-southeast precipitation pattern (typical of SAMS) is not enhanced in early and neutral onset years when LULCC is considered.

A statistically significant precipitation reduction was verified over central-east in the late onset (Figure 4q) associated with the SLP increase (Figure 4t) over the same region which reinforces the suppression of cloud formation and precipitation (Figure 4p, q). In addition, a precipitation increase was verified along the northwest, and northeast SA in the late onset year (Figure 4q). This indicates a weakening of the summer monsoon precipitation band (SACZ).

In the early onset year, precipitation was enhanced in parts of the northeast SA (Figure 4c) where a statistically significant increase of the 850 hPa wind magnitude was observed (Figure 4d). Thus, the enhanced wind magnitude (Figure 4d) contributed to the precipitation increase over these areas (Figure 4c). On the other hand, a precipitation decrease was verified over the central SA (Figure 4c). This pattern corroborates with the precipitable water decrease which does not reinforce the SACZ. Similarly, in the neutral onset year the SACZ is weakened because of the simulated precipitation decrease all over the central SA (Figure 4j).

In DJF, although the 850 hPa wind magnitude increase across the central-east SA (Figure 4d, k, r) it was lower in comparison with SON (Figure 3d, k, r). Observational data (Zilli et al., 2019) and global warming projection (Soares and Marengo, 2009) studies have associated the 850 hPa wind speed increase with the low-level jet intensification and the SACZ displacement towards the south. The results obtained here shows the SACZ intensity was affected by LULCC and its position was dependent on the considered rainy season onset year.

Similar to SON, a statistically significant 2 m temperature decrease was verified mainly over central-east and northeast in the late onset during DJF (Figure 4s), which was also verified in the potential temperature vertical profile (Figure 7). However, a statistically significant increase in 2 m temperature was observed in the central and southeast SA, especially in the neutral onset (Figure 4l) where a precipitation decrease (OLR increase) was also simulated (Figure 4i, j).

In DJF, SLP increase was observed in both early and late onset years (Figure 4f, t). In the late onset, this SLP increase was prominent in central-east SA (Figure 4t). This suggests that LULCC does not promote the typical summer monsoon pattern characterized by a reduction in SLP across the continent. Thus, it indicates that LULCC can change the SAMS features.

The areas where statistically significant reductions in net radiation were observed during DJF decreased compared to SON, primarily concentrated in the southeast SA (Figure 4g, n, u). In DJF, statistically significant increase in net radiation was verified over parts of the northeast SA (Figure 4g, n, u). Furthermore, a decrease in OLR and increase in precipitation was verified over the northeast SA (Figure 4p, q). These findings indicate that a subsequent increase in soil water content reduces the surface albedo, thus, increase the soil heat capacity. As a result, more incident shortwave radiation is absorbed, leading to an increase in surface net radiation.

Figure 5 shows a surface water budget analysis similar to the one applied by Talamoni et al. (2022), for BAM experiments over the area between 25-15°S and 50-40°W. The aim was to identify the contribution of each WB component by assessing the difference between UP and NAT experiments. In SON (Figure 5a), $C_w$ was the main contributor to the water budget of all three onset years. The moisture comes mainly from the ocean and from frontal systems. $C_w$ was greater in UP experiments of both late and neutral onset years. In addition, $C_w$ increase to the continent can be associated with the subtropical South Atlantic high-pressure system displaced closer to SA indicated by the SLP increase (Figure 3 m, t). On the other hand, the precipitation was lower in UP experiments in all years. Despite the increase in $C_w$, convective processes were inhibited due to increases in SLP associated with a dry and cold vertical profile (Figure 7).

In the early onset year, both P and $C_w$ were lower in UP experiments, resulting in a reduced WB. It can be associated with the SLP decrease over the Atlantic Ocean which contributed to inhibit the frontal systems of advancing towards the area between 25-15°S and 50-40°W, leading to a reduction in $C_w$.

The early and neutral onset years WB was higher (lower) in UP experiments in DJF (Figure 5b), mainly due to R contributions. The R increase is associated with the reduction of water absorption and interception by pasture vegetation, thereby limiting the amount of water available for soil infiltration. Additionally, E increase suggests that the exposed soil is undergoing enhanced water loss to the atmosphere.

The late onset year WB was lower in UP experiments (Figure 5b), particularly due to $C_w$ and P contributions. The $C_w$ decrease is associated with SLP increase over central-east SA and in the Atlantic Ocean (Figure 4 t) disfavours the advance of frontal systems that organizes convection and configure SACZ events. SLP increase also contribute to a more stable atmosphere (colder and drier profile in Figure 7) which supresses convection and consequently, reduces P.

## 4. Summary and Conclusions

This study investigated how LULCC affects the SA rainy season by implementing an updated vegetation map that considers the LULCC over the Brazilian territory with early 2000s deforestation rates into IBIS and BAM models. Major differences between NAT and UP vegetation maps were verified over the area between 25-15°S and 50-40°W where both Atlantic Forest and Cerrado biomes were replaced by pasture. The numerical experiments were performed with two vegetation maps (NAT and UP) on two frameworks: offline using the land-surface model (IBIS) and online using the BAM. Three rainy season onset conditions were considered in the experiments: early (2006), neutral (2004), and late (2008) rainy season onset.

In IBIS-OFFLINE experiments, similar changes in surface variables induced by LULCC were observed in all three rainy season onset years. These changes are summarized in the green boxes of the diagram in Figure 6 (based on Table 5). The shift from C3 forest to C4 pasture vegetation types (LULCC), particularly over the area between 25-15°S and 50-40°W, triggered an immediate rise in albedo (exposed land has higher albedo). Additionally, the shift led to a decrease in surface roughness due to the shorter vegetation type. As a result of these changes, more shortwave radiation is reflected by the surface, leading to a decrease in the available energy. Consequently, net radiation, surface heat fluxes (both latent and sensible), and surface temperature all decreased.

The surface-atmosphere feedback due to LULCC was assessed in BAM experiments, summarized in the pink boxes in Figure 6. While major statistically significant differences between UP and NAT experiments were observed in the late rainy season onset year and during SON, similar patterns were identified in the area 25-15°S and 50-40°W for the early and neutral onset years (Table 6). The reduction in both latent and sensible heat fluxes contributed to a decrease in precipitable water and 2 m temperature, respectively. It contributed to setting up a drier and colder (more stable) atmosphere as depicted in Figure 7. These atmospheric changes resulted in less cloud formation and reduced precipitation, accompanied by an increase in OLR. Furthermore, SLP and low-level wind increased as direct responses to the reduction in 2 m temperature and surface roughness, respectively. These results indicate that over the area where major

LULCC occurred (25-15°S and 50-40°W), the behavior of the rainy season was modified. Precipitation was suppressed through surface-atmosphere feedback mechanisms, particularly in the late rainy season onset year and SON, when there is a greater dependence on local forcing.

Overall, UP experiments exhibited a drier and colder vertical profile, with the most significant differences in the late rainy season onset during SON. This drier atmospheric profile induced by LULCC resembles the dry atmospheric condition (reduced soil moisture and precipitation, in addition to increased sensible heat flux) observed in late onset years reported by Talamoni et al. (2022) over central-east SA and by Fu and Li (2004) over the southern Amazon. Future studies can investigate the hypothesis that LULCC might delay the onset of the rainy season by amplifying the atmospheric dry pattern observed during late onset years. This hypothesis agrees with two studies that investigated the role of latent and sensible heat fluxes on SAMS development. Silva (2012) and Garcia (2010) observed surface heating over central SA preceding to the rainy season onset. This heating is important to increase both sensible and latent heat fluxes and to build up instability in the lower troposphere. From the heating, SLP decreases, promoting low-level mass convergence and upward vertical movement. In addition, we also suggest that future studies can perform long-term simulations to assess long-term changes in SAMS features.

In this study, we focused on identifying the local and non-local impacts LULCC has on both surface and atmospheric variables focusing on Brazil. In future studies, we suggest a further investigation of the mechanisms responsible for differences between NAT and UP experiments at the outskirts of the Brazilian territory. Giles et al. (2022) conducted a similar investigation, examining how soil moisture variability over southeastern South America and eastern Brazil affected the regional circulation and led to changes in precipitation over northeastern Argentina.

In conclusion, this study represents the first endeavor to incorporate an updated and realistic vegetation map of the Brazilian territory into BAM. The numerical experiments highlighted the importance of considering LULCC in vegetation maps. Therefore, we expect that future BAM experiments are performed with the UP vegetation map proposed here, and we hope this study motivates future implementations of even more realistic and up-to-date vegetation maps in AGCMs.

**Acknowledgment**

We thank two anonymous reviewers for providing helpful comments on the paper. This paper had support of *Coordenação de Aperfeiçoamento de Pessoal de Nível Superior* (CAPES). The first author (ILT) was supported by CAPES (process 88887.354679/2019-00). Acknowledgments also to CLIMAX-FAPESP-Belmont-2015/50687-8. The third author (IFAC) thanks CNPq- Project 306393/2018-2. The fifth author (JB) was supported by the European Research Council (ERC) under the European Union's Horizon 2020 research and innovation programme (DECAF project, Grant agreement No. 771492) and United Kingdom Research and Innovation (UKRI) Future Leaders Fellowship (Grant Ref: MR/X034097/1). We thank CPTEC/INPE for the technical and infrastructure support related to the Post-Graduation Program. Data was obtained from available sources as noted by references on Table 1: GLDAS, ERA5, NCEP-NOAA and GPCP.

## Conflict of interest

The authors declare no competing interests.

## Data availability

GLDAS, ERA5, RADS and GPCP were used to support the findings of this study. These datasets are all available in the public domain. GLDAS is openly available at [https://disc.gsfc.nasa.gov/datasets/GLDAS_NOAH025_M_2.1/summary?keywords=GLDAS]. ERA5 can be found at [https://doi.org/10.24381/cds.adbb2d47]. RADS is openly available at [https://climatology.tamu.edu/research/Rainy-and-Dry-Season-RADS.html#:~:text=What%20is%20RADS%3F,the%20rainy%20and%20dry%20seasons.]. GPCP can be accessed at [http://doi.org/10.7289/V56971M6]. NOAA NCEP sea surface temperature data is a product available under request at [https://www.ncei.noaa.gov/products/optimum-interpolation-sst]. The vegetation maps used in the study are available from the corresponding author upon reasonable request.

## References

Adler, R., and Coauthors, 2016: Global Precipitation Climatology Project (GPCP) Climate Data Record (CDR), Version 2.3 (Monthly). https://doi.org/10.7289/V56971M6.

Allen, R. G., Pereira, L. S., Raes, D., & Smith, M. (1998). FAO Irrigation and drainage paper No. 56. Rome: Food and Agriculture Organization of the United Nations, 56(97), e156.

Aragão, L. E. (2012). The rainforest's water pump. Nature, 489(7415), 217-218.

Araújo, A. S., de Campos Velho, H. F., & Minjiao, L. (2016). Multi-objective calibration of IBIS model by genetic algorithm with parametric sensitivity analysis. Ciência e Natura, 38, 90-97.

Beaudoing, H. and M. Rodell, NASA/GSFC/HSL (2020), GLDAS Noah Land Surface Model L4 3 hourly 0.25 x 0.25 degree V2.1, Greenbelt, Maryland, USA, Goddard

Earth Sciences Data and Information Services Center (GES DISC), Accessed: 10-03-2023, 10.5067/E7TYRXPJKWOQ.

Bombardi RJ, Kinter JL III, Frauenfeld OW (2019) A global gridded dataset of the characteristics of the rainy and dry seasons. Bull Am Meteorol Soc 100(7):1315–1328.

Bonan, G. B. (2008). Forests and climate change: forcings, feedbacks, and the climate benefits of forests. science, 320(5882), 1444-1449.

Bretherton, C. S., & Park, S. (2009). A new moist turbulence parameterization in the Community Atmosphere Model. Journal of Climate, 22(12), 3422-3448.

Brubaker, K. L., Entekhabi, D., & Eagleson, P. S. (1994). Atmospheric water vapor transport and continental hydrology over the Americas. Journal of Hydrology, 155(3-4), 407-428.

Butt, N., De Oliveira, P. A., & Costa, M. H. (2011). Evidence that deforestation affects the onset of the rainy season in Rondonia, Brazil. Journal of Geophysical Research: Atmospheres, 116(D11).

Cavalcanti, I. F. D. A., & Raia, A. (2017). Lifecycle of South American monsoon system simulated by CPTEC/INPE AGCM. International Journal of Climatology, 37, 878-896.

Chambers, J. Q., & Artaxo, P. (2017). Deforestation size influences rainfall. Nature Climate Change, 7(3), 175-176.

Chen, C. T., & Knutson, T. (2008). On the verification and comparison of extreme rainfall indices from climate models. Journal of Climate, 21(7), 1605-1621.

Chou, M. D., & Suarez, M. J. (1999). A solar radiation parameterization for atmospheric studies (No. NASA/TM-1999-104606/VOL15).

Collini EA, Berbery EH, Barros VR, Pyle ME (2008) How does soil moisture infuence the early stages of the South American monsoon? J Clim 21(2):195–213.

Cunha, A. P. M., Alvalá, R. C., Sampaio, G., Shimizu, M. H., & Costa, M. H. (2013). Calibration and validation of the integrated biosphere simulator (IBIS) for a Brazilian semiarid region. Journal of Applied Meteorology and Climatology, 52(12), 2753-2770.

Da Rocha, R. P., Morales, C. A., Cuadra, S. V., & Ambrizzi, T. (2009). Precipitation diurnal cycle and summer climatology assessment over South America: An evaluation of Regional Climate Model version 3 simulations. Journal of Geophysical Research: Atmospheres, 114(D10).

Da Silva, A. E., & de Carvalho, L. M. V. (2007). Large-scale index for South America monsoon (LISAM). Atmospheric Science Letters, 8(2), 51-57.

De Carvalho, L. M. V., & Jones, C. (2016). The monsoons and climate change (pp. 1-6). Springer.

S Debortoli, N., Dubreuil, V., Funatsu, B., Delahaye, F., de Oliveira, C. H., Rodrigues-Filho, S., ... & Fetter, R. (2015). Rainfall patterns in the Southern Amazon: a chronological perspective (1971–2010). Climatic Change, 132(2), 251-264.

Eltahir, E. A., & Bras, R. L. (1994). Precipitation recycling in the Amazon basin. Quarterly Journal of the Royal Meteorological Society, 120(518), 861-880.

Figueroa, S. N., Bonatti, J. P., Kubota, P. Y., Grell, G. A., Morrison, H., Barros, S. R., ... & Panetta, J. (2016). The Brazilian global atmospheric model (BAM): performance for tropical rainfall forecasting and sensitivity to convective scheme and horizontal resolution. Weather and Forecasting, 31(5), 1547-1572.

Foley, J. A., Prentice, I. C., Ramankutty, N., Levis, S., Pollard, D., Sitch, S., & Haxeltine, A. (1996). An integrated biosphere model of land surface processes, terrestrial carbon balance, and vegetation dynamics. Global biogeochemical cycles, 10(4), 603-628.

Fu R, Li W (2004) The influence of the land surface on the transition from dry to wet season in Amazonia. Theor Appl Climatol 78(1):97–110.

Gan, M. A., & Rao, V. B. (1991). Surface cyclogenesis over south America. Monthly Weather Review, 119(5), 1293-1302.

Gan MA, Kousky VE, Ropelewski CF (2004) The South America monsoon circulation and its relationship to rainfall over west-central Brazil. J Clim 17(1):47–66.

Garcia, S. R. Sistema de monção da América do Sul: início e fim da estação chuvosa e sua relação com a Zona de Convergência Intertropical do Atlântico. 2010. 230 p. IBI: <8JMKD3MGP8W/36STS88>. (sid.inpe.br/mtc-m18@80/2010/02.04.20.34-TDI). Tese (Doutorado em Meteorologia) - Instituto Nacional de Pesquisas Espaciais (INPE), São José dos Campos, 2010. Disponível em: <http://urlib.net/ibi/8JMKD3MGP8W/36STS88>.

Giles, J. A., C. G. Menéndez, and R. C. Ruscica, 2022: Nonlocal Impacts of Soil Moisture Variability in South America: Linking Two Land–Atmosphere Coupling Hot Spots. J. Climate, 36, 227–242, https://doi.org/10.1175/JCLI-D-21-0510.1.

Han, J., & Pan, H. L. (2011). Revision of convection and vertical diffusion schemes in the NCEP Global Forecast System. Weather and Forecasting, 26(4), 520-533.

Hersbach, H., Bell, B., Berrisford, P., Biavati, G., Horányi, A., Muñoz Sabater, J., Nicolas, J., Peubey, C., Radu, R., Rozum, I., Schepers, D., Simmons, A., Soci, C., Dee, D., Thépaut, J-N. (2023): ERA5 hourly data on single levels from 1940 to present. Copernicus Climate Change Service (C3S) Climate Data Store (CDS), DOI: 10.24381/cds.adbb2d47 (Accessed on 10-03-2023).

Huang, B., C. Liu, V. Banzon, E. Freeman, G. Graham, B. Hankins, T. Smith, and H.-M. Zhang, 2020: Improvements of the Daily Optimum Interpolation Sea Surface Temperature (DOISST) Version 2.1, Journal of Climate, 34, 2923-2939. doi: 10.1175/JCLI-D-20-0166.1

Huffman, G. J., Bolvin, D. T., Nelkin, E. J., Wolff, D. B., Adler, R. F., Gu, G., ... & Stocker, E. F. (2007). The TRMM multisatellite precipitation analysis (TMPA): Quasi-global, multiyear, combined-sensor precipitation estimates at fine scales. Journal of hydrometeorology, 8(1), 38-55.

Imbuzeiro, H. M. A. (2005). Calibração do modelo IBIS na Floresta Amazônica usando múltiplos sítios.

Khanna, J., Medvigy, D., Fueglistaler, S., & Walko, R. (2017). Regional dry-season climate changes due to three decades of Amazonian deforestation. Nature Climate Change, 7(3), 200-204.

Kodama Y (1992) Large-scale common features of subtropical precipitation zones (the Baiu frontal zone, the SPCZ, and the SACZ) Part I: characteristics of subtropical frontal zones. J Meteorol Soc Jpn Ser II 70(4):813–836.

Kousky VE (1988) Pentad outgoing longwave radiation climatology for the South American sector. Revista Brasileira De Meteorologia 3(1):217–231.

Kubota, P. Y. Variability of storage energy in the soil-canopy system and its impact on the definition of precipitation standard in South America. 2012. 285p. Thesis (PhD in Meteorology) - Instituto Nacional de Pesquisas Espaciais (INPE), São José dos Campos, Brazil, 2012.

Leite-Filho, A. T., de Sousa Pontes, V. Y., & Costa, M. H. (2019). Effects of deforestation on the onset of the rainy season and the duration of dry spells in southern Amazonia. Journal of Geophysical Research: Atmospheres, 124(10), 5268-5281.

Liebmann B, Marengo J (2001) Interannual variability of the rainy season and rainfall in the Brazilian Amazon Basin. J Clim 14(22):4308–4318.

Lima, I. T. O início da estação chuvosa na América do Sul e processos atmosféricos e de superfície associados. 2021. 177 p. IBI: <8JMKD3MGP3W34R/44478D2>. (sid.inpe.br/mtc-m21c/2021/01.29.17.06-TDI). Dissertação (Mestrado em Meteorologia) - Instituto Nacional de Pesquisas Espaciais (INPE), São José dos Campos, 2021. Disponível em: <http://urlib.net/ibi/8JMKD3MGP3W34R/44478D2>.

Ma, H. Y., Mechoso, C. R., Xue, Y., Xiao, H., Wu, C. M., Li, J. L., & De Sales, F. (2011). Impact of land surface processes on the South American warm season climate. Climate dynamics, 37(1), 187-203.

Marengo JA, Liebmann B, Grimm AM, Misra V, Silva Dias PD, Cavalcanti IFA et al (2012) Recent developments on the South American monsoon system. Int J Climatol 32(1):1.

Marengo, J. A., Cavalcanti, I. F. A., Satyamurty, P., Trosnikov, I., Nobre, C. A., Bonatti, J. P., ... & Candido, L. (2003). Assessment of regional seasonal rainfall predictability using the CPTEC/COLA atmospheric GCM. Climate Dynamics, 21(5), 459-475.

Morrison, H., Thompson, G., & Tatarskii, V. (2009). Impact of cloud microphysics on the development of trailing stratiform precipitation in a simulated squall line: Comparison of one-and two-moment schemes. Monthly weather review, 137(3), 991-1007.

Nieto-Ferreira R, Rickenbach TM (2011) Regionality of monsoon onset in South America: a three-stage conceptual model. Int J Climatol 31(9):1309–1321.

Oliveira, G. S. Conseqüências climáticas da substituição gradual da floresta tropical amazônica por pastagem degradada ou por plantação de soja: um estudo de modelagem. 2008. 417 p. IBI: <6qtX3pFwXQZGivnK2Y/TiuCH>. (INPE-15263-TDI/1346). Tese (Doutorado em Meteorologia) - Instituto Nacional de Pesquisas Espaciais (INPE), São José dos Campos, 2008. Disponível em: <http://urlib.net/ibi/6qtX3pFwXQZGivnK2Y/TiuCH>.

Raia A, Cavalcanti IFA (2008) The life cycle of the South American monsoon system. J Clim 21(23):6227–6246.

Reboita, M. S., Da Rocha, R. P., Ambrizzi, T., & Sugahara, S. (2010). South Atlantic Ocean cyclogenesis climatology simulated by regional climate model (RegCM3). Climate Dynamics, 35(7), 1331-1347.

Rezende, L. F., de Castro, A. A., Von Randow, C., Ruscica, R., Sakschewski, B., Papastefanou, P., ... & Cavalcanti, I. F. (2022). Impacts of land use change and atmospheric CO2 on gross primary productivity (GPP), evaporation, and climate in southern Amazon. Journal of Geophysical Research: Atmospheres, 127(8), e2021JD034608.

Rio, C., & Hourdin, F. (2008). A thermal plume model for the convective boundary layer: Representation of cumulus clouds. Journal of the atmospheric sciences, 65(2), 407-425.

Ruscica, R. C., Sörensson, A. A., Diaz, L. B., Vera, C., Castro, A., Papastefanou, P., ... & von Randow, C. (2022). Evapotranspiration trends and variability in southeastern South America: The roles of land-cover change and precipitation variability. International Journal of Climatology, 42(4), 2019-2038.

Satyamurty, P., da Costa, C. P. W., & Manzi, A. O. (2013). Moisture source for the Amazon Basin: a study of contrasting years. Theoretical and Applied Climatology, 111, 195-209.

Senna, M. C. A., Costa, M. H., & Pires, G. F. (2009). Vegetation-atmosphere-soil nutrient feedbacks in the Amazon for different deforestation scenarios. Journal of Geophysical Research: Atmospheres, 114(D4).

Silva, A. B. Influência dos fluxos de calor em superfície no início e no final da estação chuvosa sobre a região Centro-Oeste do Brasil. 2012. 201 p. IBI: <8JMKD3MGP7W/3CF22S2>. (sid.inpe.br/mtc-m19/2012/08.15.18.09-TDI). Dissertação (Mestrado em Meteorologia) - Instituto Nacional de Pesquisas Espaciais (INPE), São José dos Campos, 2012. Disponível em: <http://urlib.net/ibi/8JMKD3MGP7W/3CF22S2>.

Spiegel, M. R. Estatistica. Sao Paulo: McGraw-Hill do Brasil, 1979. 580p.

Soares, W. R., & Marengo, J. A. (2009). Assessments of moisture fluxes east of the Andes in South America in a global warming scenario. International Journal of Climatology: A Journal of the Royal Meteorological Society, 29(10), 1395-1414.

Souza, D. C. Consequências climáticas da desertificação parcial do semi-árido do nordeste brasileiro. 2009. 126 p. IBI: <8JMKD3MGP8W/358DHEE>. (INPE-16240-TDI/1555). Dissertação (Mestrado em Meteorologia) - Instituto Nacional de Pesquisas Espaciais (INPE), São José dos Campos, 2009. Disponível em: <http://urlib.net/ibi/8JMKD3MGP8W/358DHEE>.

SOS Mata Atlântica (2021). Relatório Anual, 2021. Available in: https://cms.sosma.org.br/wp-content/uploads/2022/07/Relatorio_21_julho.pdf. Acessed in November 1st 2022.

Spracklen, D. V., and L. Garcia-Carreras, 2015: The impact of Amazonian deforestation on Amazon basin rainfall. Geophys. Res. Lett., 42, 9546–9552, https://doi.org/10.1002/2015GL066063.

Spracklen, D. V., J. C. A. Baker, L. Garcia-Carreras, and J. Marsham, 2018: The effects of tropical vegetation on rainfall. Annu. Rev. Environ. Resour., 43, 193–218, https://doi.org/10.1146/annurev-environ-102017-030136.

Talamoni, I. L., Cavalcanti, I. F., Kubota, P. Y., de Souza, D. C., Baker, J. C., & Vieira, R. (2022). Surface and atmospheric patterns for early and late rainy season onset years in South America. Climate Dynamics, 1-16.

Taiz, L., & Zeiger, E. (2010). Plant physiology 5th Ed. Sunderland, MA: Sinauer Associates, 464.

Tarasova, T. A., & Fomin, B. A. (2000). Solar radiation absorption due to water vapor: Advanced broadband parameterizations. Journal of Applied Meteorology and Climatology, 39(11), 1947-1951.

Vera C, Higgins W, Amador J, Ambrizzi T, Garreaud R, Gochis D et al (2006) Toward a unifed view of the American monsoon systems. J Clim 19(20):4977–5000.

Vieira, R. D. S.; ALVALÁ, R. D. S.; CUNHA, A. D. A.; SESTINI, M. F.; CARVALHO, V. C.; VALERIANO, D. D. M.; SILVA, J.; ABDON, M. D. M.; PONZONI, F.; CANAVESI, V. Mapa de uso e cobertura da terra do território brasileiro para uso em modelagem climática e meteorológica. São José dos Campos: INPE, 2013. 33 p

Xie, P., Chen, M., Yang, S., Yatagai, A., Hayasaka, T., Fukushima, Y., & Liu, C. (2007). A gauge-based analysis of daily precipitation over East Asia. Journal of Hydrometeorology, 8(3), 607-626.

Xue, Y., De Sales, F., Li, W. P., Mechoso, C. R., Nobre, C. A., & Juang, H. M. (2006). Role of land surface processes in South American monsoon development. Journal of climate, 19(5), 741-762.

Xue, Y., Sellers, P. J., Kinter, J. L., & Shukla, J. (1991). A simplified biosphere model for global climate studies. Journal of climate, 4(3), 345-364.

Webster, S., Brown, A. R., Cameron, D. R., & Jones, C. P. (2003). Improvements to the representation of orography in the Met Office Unified Model. Quarterly Journal of the Royal Meteorological Society: A journal of the atmospheric sciences, applied meteorology and physical oceanography, 129(591), 1989-2010.

Wright JS, Fu R, Worden JR, Chakraborty S, Clinton NE, Risi C et al (2017) Rainforest-initiated wet season onset over the southern Amazon. Proc Natl Acad Sci 114(32):8481–8486.

Yang, Z., & Dominguez, F. (2019). Investigating land surface effects on the moisture transport over South America with a moisture tagging model. Journal of Climate, 32(19), 6627-6644.

Yu, H., Kaufman, Y. J., Chin, M., Feingold, G., Remer, L. A., Anderson, T. L., ... & Zhou, M. (2006). A review of measurement-based assessments of the aerosol direct radiative effect and forcing. Atmospheric Chemistry and Physics, 6(3), 613-666.

Zhou J, Lau KM (1998) Does a monsoon climate exist over South America? J Clim 11(5):1020–1040.

Zilli, M. T., Carvalho, L., & Lintner, B. R. (2019). The poleward shift of South Atlantic Convergence Zone in recent decades. Climate Dynamics, 52(5), 2545-2563.

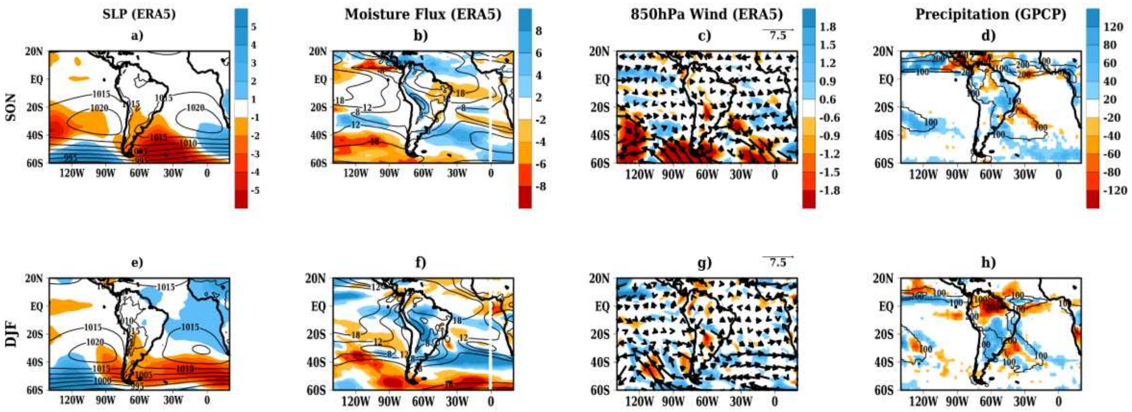


**Figure 1** – ERA5: (a)-(e) sea level pressure (shading, hPa) and climatology (contours, hPa), (b)-(f) moisture flux magnitude anomaly (shading, $10^{-5}$ kg $m^{-1}$ $s^{-1}$) and moisture flux magnitude climatology (countour, $10^{-5}$ kg $m^{-1}$ $s^{-1}$), (c)-(g) 850 hPa wind magnitude anomaly (shading, m $s^{-1}$) and vector difference (arrows, m $s^{-1}$). GPCP: (d)-(h) precipitation anomaly (shading, mm) and climatology (contour, mm). The anomaly represents the differences between the early and late onset years of SON and DJF. The climatology ranges from 1989 to 2015.

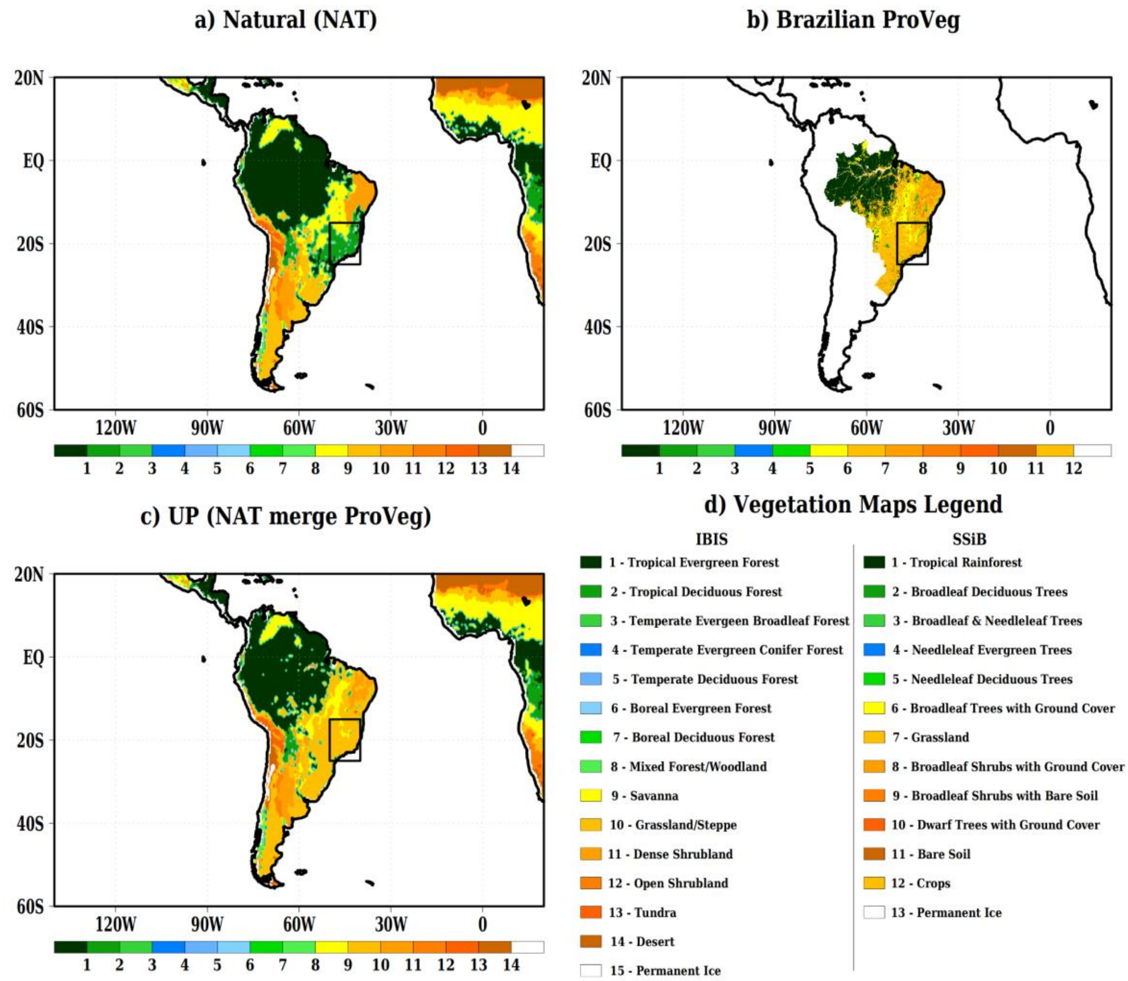


**Figure 2 –** (a) NAT vegetation map, (b) ProVeg vegetation map, (c) UP vegetation map that merges (a) and (b) to account for LULCC over the Brazilian territory. (a) and (c) are the vegetation maps used in the numerical experiments performed with IBIS and BAM. The outlined box in black is the area between (25-15°S and 50-40°W), where major LULCC occurred: Atlantic Forest (Southeast and south of Northeast regions of Brazil) and Cerrado (Central-East regions of Brazil) biomes were replaced by pasture.

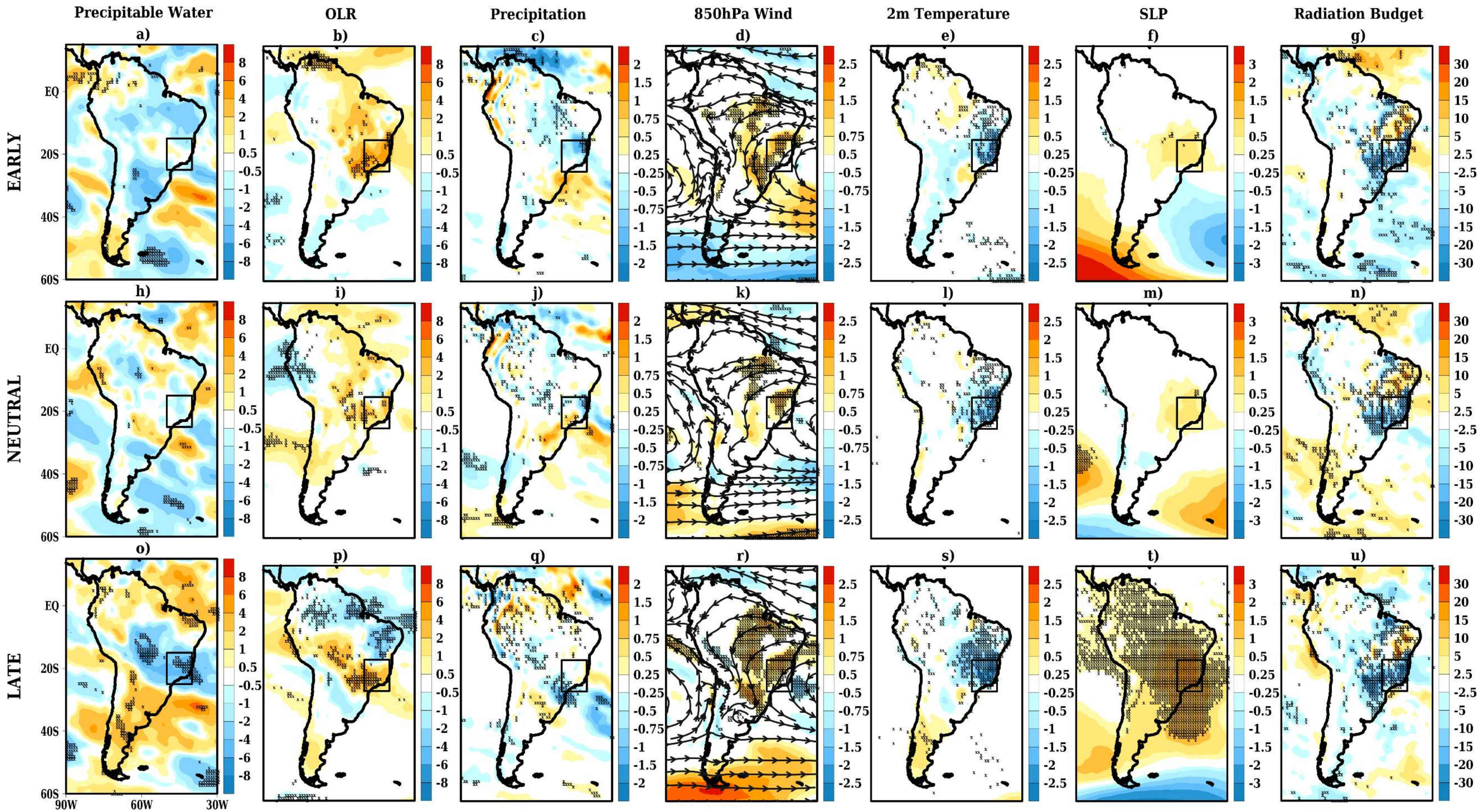


**Figure 3** – (a)-(h)-(o) precipitable water (shading), (b)-(i)-(p) OLR (shading, W m$^{-2}$), (c)-(j)-(q) precipitation (shading, mm day$^{-1}$), (d)-(k)-(r) 850 hPa wind magnitude (shading, m s$^{-1}$) and mean wind flow (streamlines), (e)-(l)-(s) 2 m temperature (shading, °C), (f)-(m)-(t) SLP (shading, hPa),

and (g)-(n)-(u) net radiation (shading, W m$^{-2}$) differences between UP and NAT experiments performed with BAM in SON at early, neutral and late rainy season onset years. Hatching areas indicate statistical significance at a 95% confidence level. The outlined box in black is the area between (25-15°S and 50-40°W), where major LULCC was identified.

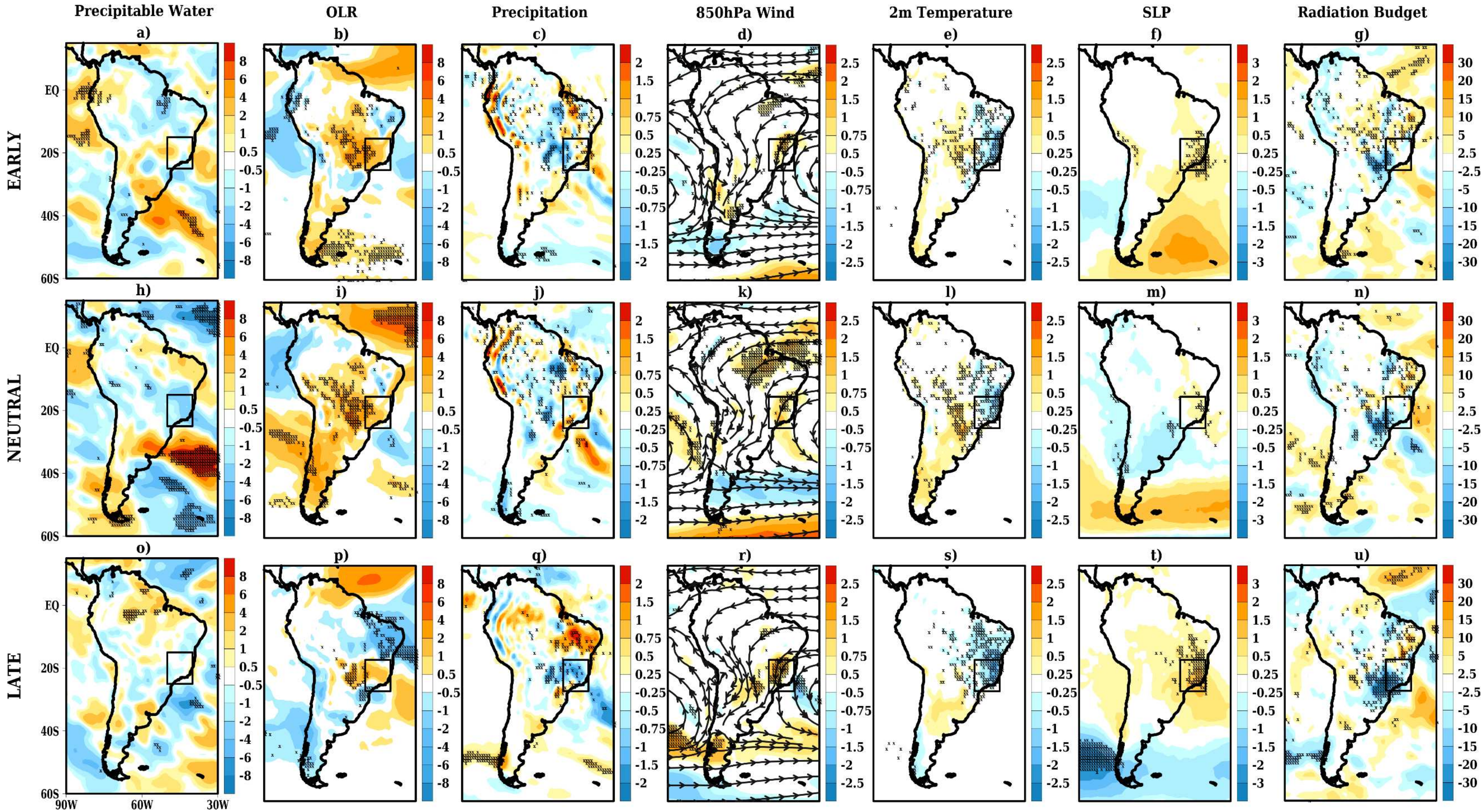


**Figure 4 -** Same as Figure 3, but in DJF.

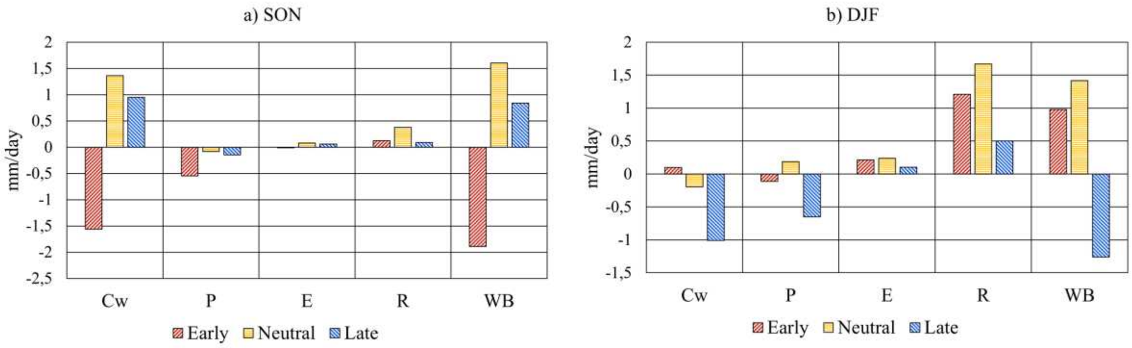


**Figure 5** – (a) SON, (b) DJF differences between UP and NAT experiments for each surface water budget component (mm day$^{-1}$) averaged over the area between 25-15°S and 50-40°W.

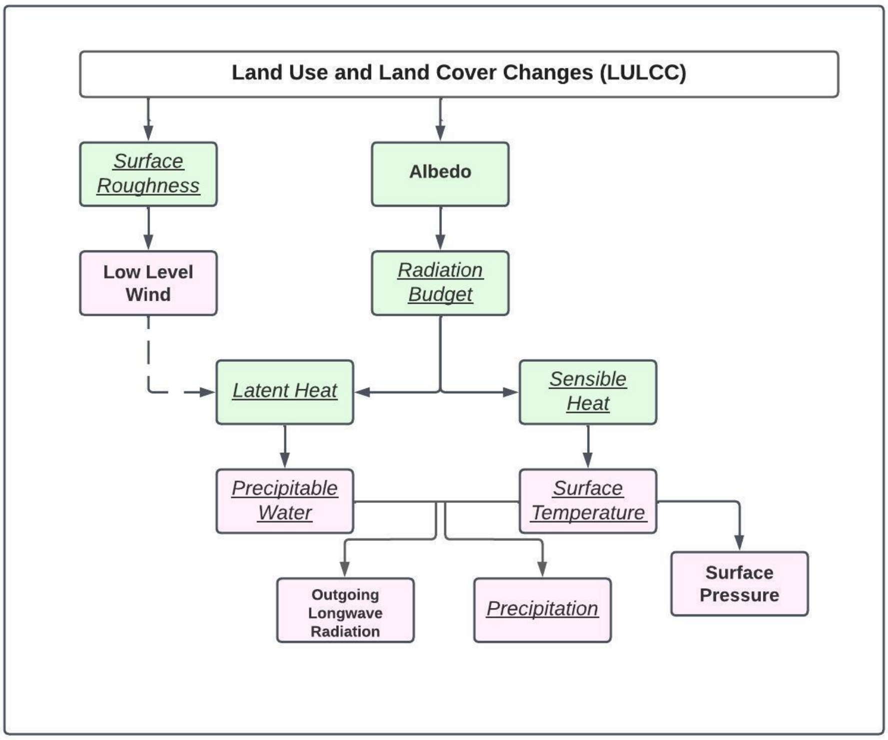


**Figure 6 -** IBIS-OFFLINE and BAM experiments variables modifications due to LULCC. Green (pink) boxes show the physical variables assessed by IBIS-OFFLINE (BAM 3D) experiments due to LULCC. The underlined (bold) variables decreased (increased) due to LULCC. The continuous (dashed) arrows indicate a positive (negative) correlation between the variables.

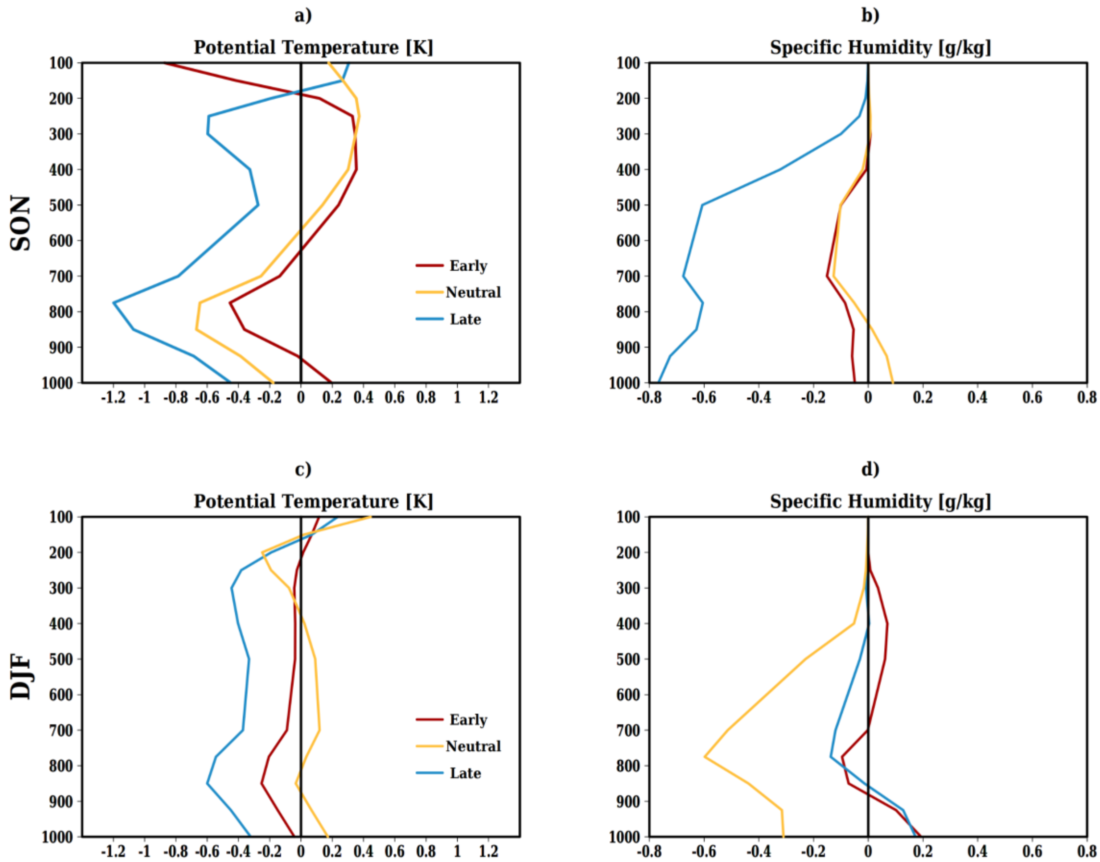


768 **Figure 7**: Vertical profile of the difference between UP and NAT (BAM) experiments
769 of (a)-(c) potential temperature (K) and (b)-(d) specific humidity (g kg$^{-1}$). The profiles
770 are averages over the area between 25-15°S and 50-40°W at both seasons SON (a, b)
771 and DJF (c, d).

| Dataset | Type | Temporal Resolution/ Coverage | Horizontal Resolution | Variables | References |
|---|---|---|---|---|---|
| GLDAS | Rain-gauge and satellite data ingested by surface modeling and data assimilation techniques | 3 hours/ July 2004 - March 2009 | 0.25° x 0.25° ~25 km | sea level pressure, precipitation, longwave incident radiation, shortwave incident radiation, temperature, surface wind, specific humidity, and soil water content | Beaudoing and Rodell (2020) |
| ERA5 | Reanalysis | Hourly/ 1981 to 2010 | 0.25° x 0.25° ~25 km | sea level pressure, U and V wind component, temperature, specific humidity and orography | Hersbach et al. (2023) |
| NCEP-NOAA | Optimum interpolation analysis using satellite and in situ data | Daily/ | 1.0° x 1.0° | Sea Surface Temperature | Huang et al. (2020) |
| GPCP | Rain-gauge and satellite data estimates | Monthly/ 1981 to 2010 | 2.5° x 2.5° | Precipitation | Adler et al. (2016) |

**Table 1:** Data description used in this study. ERA5 dataset has 37 vertical levels.

| Exp. | Onset Condition | Simulation Period | Vegetation Map |
|---|---|---|---|
| E01 | Early Year | 01/07/2006 - 28/02/2007 | NAT |
| N01 | Neutral Year | 01/07/2004 - 28/02/2005 | |
| L01 | Late Year | 01/07/2008 - 28/02/2009 | |
| E02 | Early Year | 01/07/2006 - 28/02/2007 | UP |
| N02 | Neutral Year | 01/07/2004 - 28/02/2005 | |
| L02 | Late Year | 01/07/2008 - 28/02/2009 | |

**Table 2**: IBIS-OFFLINE experiments. Hourly output frequency and continuous simulations.

| Physical Process | Configuration |
|---|---|
| Cloud Microphysics | Double-moment microphysics scheme (Morrison et al., 2009) |
| Land surface | Dynamic vegetation model - IBIS v.2.6 (Foley et al., 1996), implemented and adapted by Kubota (2012) |
| Shortwave radiation | CLIRAD-SW (Chou and Soarez, 1999) modified by Tarasova and Fomin, 2000 |
| Longwave radiation | CLIRAD-LW (Chou et al., 2001) |
| Planetary Boundary Layer (PBL) | Turbulence scheme for vertical diffusion of momentum, heat, and moisture (Bretherton and Park, 2009) |
| Deep convection | Arakawa-Schubert simplified and reviewed (Han and Pan, 2011) |
| Aerosol optical depth | Yu et al. (2006) |
| Thermal plume for PBL | Rio and Hourdin (2008) |
| Gravity wave drag | Webster et al.'s (2003) scheme with low-level blocking |

**Table 3:** Physical processes configurations of BAM v.2.2.1.

| Exp. | Initial Condition Date | Simulation Period | Exp. | Initial Condition Date | Simulation Period |
|---|---|---|---|---|---|
| **Early Onset - 2006** | | | | | |
| C1.1 | 2006 07 **01** 12 | July - March | C1.6 | 2006 10 **01** 12 | October - May |
| C1.2 | 2006 07 **02** 12 | | C1.7 | 2006 10 **02** 12 | |
| C1.3 | 2006 07 **03** 12 | | C1.8 | 2006 10 **03** 12 | |
| C1.4 | 2006 07 **04** 12 | | C1.9 | 2006 10 **04** 12 | |
| C1.5 | 2006 07 **05** 12 | | C1.10 | 2006 10 **05** 12 | |
| **Neutral Onset - 2004** | | | | | |
| C2.1 | 2004 07 **01** 12 | July - March | C2.6 | 2004 10 **01** 12 | October - May |
| C2.2 | 2004 07 **02** 12 | | C2.7 | 2004 10 **02** 12 | |
| C2.3 | 2004 07 **03** 12 | | C2.8 | 2004 10 **03** 12 | |
| C2.4 | 2004 07 **04** 12 | | C2.9 | 2004 10 **04** 12 | |
| C2.5 | 2004 07 **05** 12 | | C2.10 | 2004 10 **05** 12 | |
| **Late Onset - 2008** | | | | | |
| C3.1 | 2008 07 **01** 12 | July - March | C3.6 | 2008 10 **01** 12 | October - May |
| C3.2 | 2008 07 **02** 12 | | C3.7 | 2008 10 **02** 12 | |
| C3.3 | 2008 07 **03** 12 | | C3.8 | 2008 10 **03** 12 | |
| C3.4 | 2008 07 **04** 12 | | C3.9 | 2008 10 **04** 12 | |
| C3.5 | 2008 07 **05** 12 | | C3.10 | 2008 10 **05** 12 | |

**Table 4:** BAM experiments design. A 2-month spin-up was considered for each simulation period. Monthly output frequency experiments. The initial condition date is in the format year/month/day/hour.

| Surface Variables | UP - NAT (SON) | | | UP - NAT (DJF) | | |
|---|---|---|---|---|---|---|
| | Early | Neutral | Late | Early | Neutral | Late |
| Albedo | 0,088 | 0,083 | 0,084 | 0,080 | 0,079 | 0,081 |
| Latent heat flux (W $m^{-2}$) | -14,09 | -9,51 | -8,58 | -11,98 | -16,47 | -12,20 |
| Sensible heat flux (W $m^{-2}$) | -17,28 | -25,78 | -25,01 | -14,94 | -14,61 | -17,65 |
| Net radiation (W $m^{-2}$) | -17,17 | -20,35 | -20,32 | -16,06 | -17,13 | -21,17 |
| Soil water content | -0,006 | -0,002 | -0,001 | 0,004 | -0,006 | -0,003 |
| Surface Temperature (°C) | -0,24 | -0,02 | -0,05 | -0,16 | -0,17 | 0,10 |

**Table 5:** Mean difference between UP and NAT (IBIS OFFLINE) experiments over the area between 25-15°S and 50-40°W in SON and DJF. Highlighted in blue (red) are the negative (positive) differences which represent a decrease (increase) of the respective surface parameter in UP experiment compared to NAT experiment.

| Atmospheric Variables | UP - NAT (SON) | | | UP - NAT (DJF) | | |
|---|---|---|---|---|---|---|
| | Early | Neutral | Late | Early | Neutral | Late |
| Precipitable water (mm $day^{-1}$) | -0,52 | -0,47 | -4,21 | 0,21 | -1,98 | -0,20 |
| Outgoing Longwave Radiation (W $m^{-2}$) | 3,56 | 1,21 | 2,09 | 1,28 | 1,01 | 0,60 |
| Precipitation (mm $day^{-1}$) | -0,55 | -0,06 | -0,19 | -0,11 | 0,19 | -0,65 |
| Sea Level Pressure (hPa) | 0,53 | 0,51 | 1,47 | 0,51 | 0,21 | 0,92 |
| 850hPa wind speed (m $s^{-1}$) | 0,64 | 0,66 | 0,77 | 0,55 | 0,82 | 0,71 |
| Surface Temperature (°C) | -0,91 | -1,09 | -1,32 | -0,48 | -0,36 | -0,73 |
| Net Radiation (W $m^{-2}$) | -10,41 | -9,18 | -10,40 | -1,30 | -3,06 | -7,57 |

**Table 6:** Mean difference between UP and NAT (BAM) experiments over the area between 25-15°S and 50-40°W in SON and DJF. Highlighted in blue (red) are the negative (positive) differences which represent a decrease (increase) of the respective atmospheric parameter in UP experiment compared to NAT experiment.